

# Impact Phenomena in a Non-Contacting Mechanical Face Seal

**Philip Varney \***

Graduate Research Assistant  
Woodruff School of Mechanical Engineering  
Georgia Institute of Technology  
Atlanta, Georgia, 30318  
Email: pvarney3@gatech.edu

**Itzhak Green**

Professor  
Woodruff School of Mechanical Engineering  
Georgia Institute of Technology  
Atlanta, Georgia, 30318  
Email: itzhak.green@me.gatech.edu

## ABSTRACT

**Abstract:** Non-contacting mechanical face seals are often described as unpredictable machine elements, gaining this moniker from numerous instances of premature and unexpected failure. Machine faults such as misalignment or imbalance exacerbate seal vibration, leading to undesirable and unforeseen contact between the seal faces. A hypothesis explaining the high probability of failure in non-contacting mechanical face seals is this undesired seal face contact. However, research supporting this hypothesis is heuristic and experiential, and lacks the rigor provided by robust simulation incorporating contact into the seal dynamics. Here, recent developments in modeling rotor-stator rub using rough surface contact are employed to simulate impact phenomena in a flexibly-mounted stator mechanical face seal designed to operate in a non-contacting regime. Specifically, the elastoplastic Jackson-Green rough surface contact model is used to quantify the contact forces using real and measurable surface and material parameters. This method also ensures that the seal face clearance remains positive, thus allowing one to calculate fluid film forces. The seal equations of motion are simulated to indicate several modes of contacting operation, where contact is identified using waveforms, frequency spectra, and contact force calculations. Interestingly, and for the first time, certain parameters generating contact are shown to induce aperiodic mechanical face seal vibration, which is a useful machine vibration monitoring symptom. Also for the first time, this work analytically shows a mechanism where severe contact precipitates seal failure, which was previously known only through intuition and/or experience. The utility of seal face contact diagnostics is discussed along with directions for future work.

## 1 Introduction

Mechanical face seals separate high and low pressure fluid reservoirs while simultaneously allowing a rotating shaft to transmit power across the interface. The high and low pressure fluid reservoirs are sealed by restricting flow across the interface, which can be accomplished using several different seal designs. In the simpler case, fluid sealing is realized using continuous contact between the seal faces [1–3], which essentially reduces leakage to zero. However, operating with continuous contact also generates undesirable wear and adverse thermal stresses [4, 5]. Consequentially, contacting mechanical face seals have a finite life and cause the operator to incur significant replacement costs.

Other applications require fluid-film mechanical face seals, such as nuclear power plant primary coolant pumps [6] and high-performance turbomachines [7]. These non-contacting mechanical face seals operate with sealing interface clearances which are typically greater than several standard deviations of surface roughness. By separating the faces using fluid lubrication, contact is hypothetically avoided during normal operation. However, this theoretically infinite design life is realized

---

\*Corresponding author.

at the expense of leakage and component simplicity. Regarding complexity, properly designing a non-contacting mechanical face seal requires knowledge of, for example, fluid film lubrication [8, 9], seal dynamics [1, 10], surface roughness [11, 12], and thermal effects [11–13]. A specific seal design proficient at avoiding occasional face contact is the near-contact mechanical face seal, where surface texturing generates large axial fluid film stiffness at dangerously small clearances [14].

Though non-contacting mechanical face seals have theoretically infinite design lives, these components often fail prematurely and without warning. A possible explanation for premature failure is unexpected contact between the seal faces [15, 16], which were designed to operate in non-contacting regimes. Contact can be caused by many effects, such as inadequate lubrication, excessive vibration, large misalignments between the faces [15, 16], or transient operation [12, 17]. Mitigating undesired face contact requires seal redesign and real-time condition monitoring to detect the onset of face contact. Most previous studies focus on detecting contact experimentally using methods such as vibration monitoring [15, 16, 18], ultrasonic techniques [19–21], acoustic emission [22, 23] or a combination of methods [24]. Others have used these same experimental measurement techniques to heuristically identify contact signatures and apply these signatures to an actively-controlled seal in an attempt to eliminate contact [25–28].

A better analytic understanding of mechanical face seal contact would provide useful information for detecting contact and improving seal designs. Green [12] models a flexibly-mounted stator (FMS) mechanical face seal and incorporates contact forces during transient start-up (i.e., lift-off) and shut-down operation using the elastoplastic Chang-Etsion-Bogy [29] rough surface contact model. Still, contact is only considered as a transient phenomena, and contact during steady-state operation is not considered. Furthermore, the focus of the work is presenting seal performance metrics rather than dynamic signatures of face contact. Other works have considered asperity contact forces in mechanical face seals when analyzing the lubrication problem [30], but do not extend the analysis to the system's dynamic behavior.

The objective here is to study contact in a FMS mechanical face seal as an intermittent phenomenon occurring at steady-state operation. The FMS configuration [10, 31] is used herein due to its simplicity, even though the more complex flexibly-mounted rotor configuration has previously been shown to be stable for all operating regimes [32, 33]. Specifically, the FMS seal response to contact is shown using tilt waveforms, frequency spectra, and contact force calculations. Several cases are investigated, including the no-contact condition for comparison, light contact along the inner radius, heavy contact, and failure of a flat-faced seal via instability-induced severe contact.

## 2 FMS Mechanical Face Seal Modeling

The flexibly-mounted stator (FMS) mechanical face seal is shown schematically in Fig. 1. The non-rotating seal ring is flexibly-mounted to the housing via two elastic components: a radial support spring and a viscoelastic secondary seal O-ring. The radial support spring stiffness is selected, along with the inner, outer, and balance radii, to provide a desired set-point clearance  $C_0$  between the seal ring and rotating seal seat (i.e., the rotor). Face coning is used on the seal ring to create a converging gap between the high and low pressure reservoirs, at  $P_o$  and  $P_i$ , respectively. This converging gap creates a substantial fluid pressure profile within the sealing dam, which in turn is responsible for both sealing and seal lift-off (i.e., separation between the faces).

### 2.1 System Modeling

The flexibly-mounted seal element is free to tilt about the inertial  $\xi\eta\zeta$  axes (see Fig. 2, where  $\xi$  and  $\zeta$  define the inertial frame without showing  $\eta$  for brevity), and translate in the  $\zeta$  direction; these three degrees of freedom are denoted  $\gamma_\xi$ ,  $\gamma_\eta$ , and  $u_z$ , respectively. The rotating element rotates at a constant rate of  $n$ . A fixed coning angle  $\beta$  forms on the face of the primary seal element (i.e., the FMS) from thermal and mechanical deformations [12]; for simplicity, this work assumes the coning to be fixed and constant. The elastomeric secondary seal has stiffness and damping coefficients  $K_{sz}$  and  $D_{sz}$  and is located a radial distance  $r_s$  from the centerline; these quantities are used to find the angular stiffness and damping coefficients  $K_s$  and  $D_s$  [34]. The mass and transverse mass moment of inertia of the FMS are  $m$  and  $I_t$ , respectively.

Seal face misalignment and rotor run-out are generated by inevitable finite manufacturing tolerances and installation imperfections, and then aggravated by mechanical and/or thermal effects over the component's life time. The rotor run-out tilt magnitude is denoted  $\gamma_r$ , and is assumed to be constant in this work. The kinematic constraint between the seal faces is originally provided by Green and Etsion [10] and expounded upon in greater detail by Green [35]. Using this kinematic constraint, Green and Etsion [10] provide the equations of motion in a FMS-fixed reference frame. In the inertial frame,

these equations of motion become

$$I_t \ddot{\gamma}_\xi + D_s \dot{\gamma}_\xi + K_s \gamma_\xi = K_s \gamma_{si} + \int_0^{2\pi} \int_{r_i}^{r_o} P(r, \theta, t) r^2 \sin \theta \, dr \, d\theta \quad (1)$$

$$I_t \ddot{\gamma}_\eta + D_s \dot{\gamma}_\eta + K_s \gamma_\eta = - \int_0^{2\pi} \int_{r_i}^{r_o} P(r, \theta, t) r^2 \cos \theta \, dr \, d\theta \quad (2)$$

$$m \ddot{u}_z + D_{sz} \dot{u}_z + K_{sz} u_z = \int_0^{2\pi} \int_{r_i}^{r_o} P(r, \theta, t) r \, dr \, d\theta - F_{cls} \quad (3)$$

where  $r_o$  and  $r_i$  are the inner and outer radii of the FMS,  $P(r, \theta, t)$  is the pressure profile within the sealing dam (due to fluid forces and asperity contact), and  $F_{cls}$  is the closing force generated by the support spring and pressure forces. Static misalignment tilt of the stator is unavoidable in practical situations, and is represented here by  $\gamma_{si}$ ; this static misalignment is assumed to occur about the  $\xi$  axis without any loss of generality. Interestingly, the static misalignment serves much the same purpose as gravity in lateral rotor contact scenarios [36], as it creates an asymmetric proclivity for contact along the seal circumference. Locations within the sealing dam are referenced using coordinates  $r$  and  $\theta$ , where  $r$  is defined from the shaft centerline and  $\theta$  is defined positive counter-clockwise from  $\xi$  (see Fig. 2).

The FMS tilts  $\gamma_\xi$  and  $\gamma_\eta$  are related kinematically to the stator tilt magnitude  $\gamma_s$  and precession  $\psi_s$  by the following:

$$\gamma_\xi = \gamma_s \cos \psi_s \quad (4)$$

$$\gamma_\eta = \gamma_s \sin \psi_s \quad (5)$$

Thus, once the equations of motion are solved numerically, the total tilt and precession of the stator are found to be  $\gamma_s = \sqrt{\gamma_\xi^2 + \gamma_\eta^2}$  and  $\tan \psi_s = \gamma_\eta / \gamma_\xi$ . As will be seen, the fluid pressure depends not only on the fluid film thickness magnitude, but also the rate at which the film thickness changes. Equations 4 and 5 are differentiated to yield

$$\dot{\gamma}_\xi = \dot{\gamma}_s \cos \psi_s - \gamma_s \dot{\psi}_s \sin \psi_s \quad (6)$$

$$\dot{\gamma}_\eta = \dot{\gamma}_s \sin \psi_s + \gamma_s \dot{\psi}_s \cos \psi_s \quad (7)$$

Once the equations of motion are solved at each time step for  $\gamma_\xi$ ,  $\dot{\gamma}_\xi$ ,  $\gamma_\eta$ , and  $\dot{\gamma}_\eta$ , Eqs. 6 and 7 are solved to find  $\dot{\gamma}_s$  and  $\dot{\psi}_s$ :

$$\dot{\gamma}_s = \dot{\gamma}_\xi \cos \psi_s + \dot{\gamma}_\eta \sin \psi_s \quad (8)$$

$$\dot{\psi}_s = \frac{1}{\gamma_s} [\dot{\gamma}_\eta \cos \psi_s - \dot{\gamma}_\xi \sin \psi_s] \quad (9)$$

Clearly, the relative clearance between the rotor and stator is the parameter dictating the onset of contact. Since the tilts of the rotor and stator are small, the relative tilt  $\bar{\gamma}^*$  between the faces is

$$\bar{\gamma}^* = \bar{\gamma}_s - \bar{\gamma}_r \quad (10)$$

The magnitude of this vectorial sum is

$$(\bar{\gamma}^*)^2 = \gamma_s^2 + \gamma_r^2 - 2\gamma_s \gamma_r \cos(\psi_s - \psi_r) \quad (11)$$

## 2.2 Sealing Dam Clearance

The film thickness within the sealing dam, i.e., between the flexibly mounted stator element and the seal seat, is given by

$$h(r, \theta, t) = C_0 + u_z + \gamma_s r \sin(\theta - \psi_s) - \gamma_r r \sin(\theta - \psi_r) + \beta(r - r_i) \quad (12)$$

The axial deflection of the FMS,  $u_z$ , is referenced relative to the desired set-point clearance  $C_0$ . Evaluating derivatives with respect to circumferential position  $\theta$  and also time will prove useful when deriving the hydrodynamic forces between the seal faces:

$$\frac{\partial h}{\partial \theta} = \gamma_s r \cos(\theta - \psi_s) - \gamma_r r \cos(\theta - \psi_r) \quad (13)$$

$$\begin{aligned} \frac{\partial h}{\partial t} = & \dot{u}_z + \dot{\gamma}_s r \sin(\theta - \psi_s) - \dot{\psi}_s \gamma_s r \cos(\theta - \psi_s) \\ & - \dot{\gamma}_r r \sin(\theta - \psi_r) + \dot{\psi}_r \gamma_r r \cos(\theta - \psi_r) \end{aligned} \quad (14)$$

Here, the rotor run-out magnitude  $\gamma_r$  is not time-dependent; i.e.,  $\dot{\gamma}_r = 0$ . Furthermore, the rate at which the rotor precession changes,  $\dot{\psi}_r$ , is merely the shaft speed  $n$ .

### 2.3 Fluid Pressure

The seal is designed to operate at a specific set-point clearance  $C_0$ ; obtaining this clearance requires balancing the opening and closing forces on the flexibly mounted element. The opening force is generated solely by fluid pressure between within the sealing dam, while the closing force is generated by both the radially-mounted spring and fluid forces on the backside of the stationary seal ring. The static pressure profile has been solved from the Reynolds equation using the narrow seal approximation [8]:

$$P_s(r, \theta) = P_0 - (P_0 - P_i) \frac{h_i^2}{h_0^2 - h_i^2} \left[ \left( \frac{h_0}{h} \right)^2 - 1 \right] \quad (15)$$

where the subscripts ‘o’ and ‘i’ represent outer and inner parameters, respectively. Integrating this axisymmetric static pressure profile across the sealing dam area provides the fluid film opening force:

$$F_o = 2\pi \int_{r_i}^{r_o} P_s(r) r dr \quad (16)$$

The closing force is a summation of the spring force,  $F_{spr}$  and the pressure forces acting on the seal ring backside:

$$F_{cls} = F_{spr} + \pi [P_o(r_o^2 - r_b^2) + P_i(r_b^2 - r_i^2)] \quad (17)$$

In this work, the spring force is assumed to be constant ( $F_{spr} \neq F_{spr}(u_z)$ ) since the axial deflections are small. These equations are then used to select a balance radius  $r_b$  yielding the desired set-point clearance  $C_0$ .

Seal face misalignment and rotor rotation result in hydrodynamic fluid film forces across the sealing dam. The hydrodynamic pressure profile is found by analytically solving the isoviscous Reynolds Equation using the narrow-seal approximation [9, 37, 38]:

$$P_d(r, \theta, t) = -3\mu \left( n \frac{\partial h}{\partial \theta} + 2 \frac{\partial h}{\partial t} \right) \frac{(r_o - r)(r - r_i)}{h_m h^2} \quad (18)$$

where  $h_m = h(r_m, \theta)$ , and  $r_m$  is the mean seal ring radius. For the parameters given in Appendix A, the narrow seal approximation results in less than 2% error in the fluid film force calculations [9]. The total fluid pressure  $P_f(r, \theta, t)$  is the sum of the hydrostatic (Eq. 15) and hydrodynamic (Eq. 18) components:

$$P_f(r, \theta, t) = P_s(r, \theta, t) + P_d(r, \theta, t) \quad (19)$$

To account for cavitation, any fluid pressure less than zero is set equal to zero. Though simple, this cavitation model promotes computational expediency over small improvements in accuracy, as more advanced cavitation models [39] require solving the Reynolds equation numerically at each simulation time step.

The fluid pressure approximation used here is unaffected by the presence of surface roughness. As shown experimentally by Bair et al., [40], that even under excessive contact, the ratio of real to apparent contact area is extremely small. Furthermore, Green [12] shows that: (a) in mechanical seals, because of tilt, contact is highly limited and localized to a very small region on the seal faces, and (b) by design mechanical seals are inherently balanced [25] and the net contact loading is trifling, i.e., by and large at the region of contact, the ratio ( $h/\sigma \approx 3$ ), while being much larger elsewhere. These considerations negate the effects of the flow factors approach introduced by Patir and Cheng [41]. That is, lubrication and contact can be regarded as decoupled phenomena.

## 2.4 Contact Pressure

In reality, real surfaces are composed of peaks and valleys known as asperities. In the same manner as the elastic Greenwood-Williamson model [42], the contact of two opposing rough surfaces is reduced to that of one rigid flat contacting a single composite rough surface (see Fig. 3). The asperity heights  $z$  are defined from the mean asperity height, where  $y_s$  is the distance between the mean surface height and the mean asperity height [43]. The standard deviation of surface heights and asperity heights are  $\sigma$  and  $\sigma_s$ , respectively, the composite areal asperity density is  $N$ , and  $R_a$  is the composite average asperity radius of curvature [42]. Here, the asperity heights are assumed to obey a Gaussian distribution  $\phi(z)$ :

$$\phi(z/\sigma) = \frac{1}{\sqrt{2\pi}} \left( \frac{\sigma}{\sigma_s} \right) \exp \left[ -0.5 \left( \frac{\sigma}{\sigma_s} \right)^2 (z/\sigma)^2 \right] \quad (20)$$

Jackson and Green [44] extend a finite element study of flattening elastoplastic hemispherical contact to rough surface contact, and show that hardness is a function of geometry and material properties [45]. The interference between each asperity and the contacting rigid flat is  $\omega = z - d$ , where  $d$  is the general surface separation distance (here,  $d = h(r, \theta, t) - y_s$ ). The critical interference  $\omega_c$  denotes the interference at which yielding occurs, with a critical contact force at yielding of Using the critical interference, the contact force at the point of initial yielding is

$$\bar{F}_{cy} = \frac{4}{3} \left( \frac{R}{E} \right)^2 \left( \frac{1}{2} \pi C S_y \right)^3 \quad (21)$$

where the over-bar denotes quantities provided for single-asperity contact. The material Poisson ratio is  $\nu$  and the yield strength is  $S_y$ . Specifically, the product  $C S_y$  is chosen as  $C S_y = \min(C(\nu_1) S_{y1}, C(\nu_2) S_{y2})$  [46], where in this work surfaces 1 and 2 represent the primary seal ring and seal seat. The yield strength  $S_y$  is found from the plasticity index [45], while  $C$  is calculated according to Green [46]. Here,  $E$  is the composite elastic modulus for the contacting surfaces [42]. For small deformations,  $0 \leq \omega/\omega_c \leq 1.9\omega_c$ , the solution is essentially identical to the Hertzian model. For  $\omega > 1.9\omega_c$ , the contact force acting on a single asperity is

$$\bar{F} = \bar{F}_{cy} \left\{ \left[ \exp \left( -\frac{1}{4} \left( \frac{\omega}{\omega_c} \right)^{5/12} \right) \right] \left( \frac{\omega}{\omega_c} \right)^{3/2} + \frac{4H_G}{C S_y} \left[ 1 - \exp \left( -\frac{1}{25} \left( \frac{\omega}{\omega_c} \right)^{5/9} \right) \right] \left( \frac{\omega}{\omega_c} \right) \right\} \quad (22)$$

where

$$H_G = 2.84 C S_y \left[ 1 - \exp \left( -0.82 \left( \sqrt{\frac{\omega}{R}} \left( \frac{\omega}{1.9\omega_c} \right)^{\frac{B}{2}} \right)^{-0.7} \right) \right] \quad (23)$$

The quantity  $B$  is provided by Varney and Green [43]. Equation 23 indicates that surface hardness  $H_G$  depends on both material and surface properties along with deformation magnitudes. Still, Eq. 23 only provides the contact force acting on a single asperity.

In the current work, when the rigid flat and composite rough surface are separated by a distance  $d = h(r, \theta, t) - y_s$ , any asperity whose height exceeds  $h(r, \theta, t)$  contacts the rigid flat. Thus, the contribution of all asperities of height  $z$  towards the total contact force at circumferential location  $\theta$  is

$$\tilde{F}(z, \theta) = N A_n \bar{F}(z - d) \phi(z) \quad (24)$$

where  $A_n$  is the nominal contact area. Thus, the total contact force at a prescribed surface separation distance is found by summing the contribution of all asperities whose height exceeds the surface separation distance. This summation is achieved by integrating Eq. 24 over the entire vertical contact range (i.e., all asperity heights above  $d$ ):

$$F(\theta) = NA_n \int_d^\infty \bar{F}(z-d)\phi(z) dz \quad (25)$$

Since in this work the film thickness  $h(r, \theta, t)$  is a function of circumferential and radial location, Eq. 25 is evaluated separately at each nodal point  $(r, \theta)$ . Rather than evaluate the nominal contact area  $A_n$  at each simulation time step, Eq. 25 is redefined to calculate the average contact pressure,  $P_c(r, \theta, t) = F(r, \theta, t)/A_n$ :

$$P_c(r, \theta, t) = N \int_d^\infty \bar{F}(z-d)\phi(z) dz \quad (26)$$

Note that the contact force considered herein is quasistatic in that inertial effects at the asperities are neglected; therefore, the contact force only depends on the clearance between the seal faces. For expediency in numerically integrating the equations of motion, an exponential curve fit is performed on contact pressure  $P_c$  versus film thickness  $h$  (the approach has been documented by Varney and Green [43]); this method dramatically reduces computation time in that the numeric integration in Eq. 26 is performed only once, rather than at every nodal point  $(r, \theta)$  at every time step. Now, integrating the total pressure

$$P(r, \theta, t) = P_f(r, \theta, t) + P_c(r, \theta, t) \quad (27)$$

over the seal ring area as per Eqs. 1 - 3 provides the forces and moments generated by the fluid film and asperity contact.

### 3 Results

The equations of motion, Eqs. 1 - 3, are integrated numerically using MATLAB®'s implicit variable-step ordinary differential equation solver, ode15s. The integration tolerances must be carefully selected due to small rotor-seal interferences; here, the relative and absolute tolerances are set to  $10^{-9}$  and  $10^{-13}$ , respectively. Appropriate tolerances are selected by progressively tightening the tolerance until convergence is obtained. The initial conditions are selected to be  $\gamma_{\xi,0} = \gamma_r$  while setting all other initial conditions to zero. Time has been normalized by the shaft speed,  $n$ , such that the non-dimensional time is given by  $\tau = nt$ . A consequence of the temporal normalization is a commensurate normalization of the frequency spectra by  $n$  (hence, the synchronous component occurs at a value of 1 rather than the dimensional  $n$ ). The seal and surface parameters used here are tabulated in Appendix A, unless otherwise noted. The rough surface model parameters used herein have been calculated previously from real surface measurements [44]. The fluid and contact pressures are evaluated practically by discretizing the seal face surface into  $N_\theta$  and  $N_r$  nodes in the circumferential and radial directions.

#### 3.1 Validation

The system model and numeric solution procedure is validated, without considering contact, by comparing to previous results given by Green and Etsion [10] (the parameters used in the validation are provided therein). The results from the validation are shown in Fig. 4, where the normalized relative tilt (Eq. 11) is shown versus normalized rotor run-out  $\gamma_r$  for several representative shaft speeds. The calculated results closely follow the trends given by Green and Etsion [10], with some allowance made for parameters not provided in the original work.

#### 3.2 Contacting Seal Results

An example of light contact between the seal faces is shown in Figs. 5 and 6 for a coned-face FMS seal (see Appendix A for system and surface parameters). For comparison, the commensurate case without contact is also displayed in Fig. 5, where contact is removed by reducing the surface height standard deviation  $\sigma$  (it is merely coincidental that the lower envelope of the no-contact case appears to intersect the  $3\sigma$  boundary). Interestingly, the minimum film thickness waveforms shown in Fig. 5a are qualitatively similar even when contact exists between the faces, and only differ in amplitude and offset. The frequency spectra of both responses, Fig. 5b, are practically indistinguishable (where the half-frequency whirl shown in a result of the fluid film pressure [38]).

This similarity is explained by the seal geometry and the primary function of a flexibly-mounted seal element. First, as shown in Fig. 6a, contact between the seal faces is geographically-limited by the coning induced face taper. Even though

large contact pressures are generated, the small contact area results in small contact forces and moments when compared to those resulting from the fluid film (see Fig. 6b). A second explanation for the qualitative similarity in waveform shape is gleaned from the primary function of a flexibly-mounted seal element. In conventional rotor-stator rub situations [36], the stator and rotor motions are decoupled except when contact occurs. In the case of a flexibly-mounted seal element, however, the lubrication couples the seal rings, while the support elasticity allows the flexibly-mounted element to track the misaligned element [34, 47, 48]; this tracking phenomenon acts to continuously attempt to minimize the relative tilt between the seal faces. These two effects, localized contact regions and seal face misalignment tracking, serve to minimize the rich nonlinear responses often observed in rotor-stator systems experiencing lateral contact. Importantly, this implies that detecting seal face contact via conventional methods, such as acoustic emission or vibration monitoring, may be very difficult for light contact conditions. Thus, light contact can persist for some time in such a situation, and the locally-high contact pressures could cause significant surface wear prior to detection.

An example of heavy contact between the seal faces is shown in Fig. 7, where the minimum film thickness and frequency spectra are used to indicate contact. In this case, the response is characterized by rich nonlinear phenomena in the frequency domain, angular tilt orbit, and Poincaré section (the Poincaré return points are obtained by stroboscopically sampling the response every  $2\pi$  nondimensional units of time). Here, the frequency domain displays a significant number of harmonics, which along with scattering in the Poincaré section, indicates aperiodic seal motion. The appearance of these symptoms during seal operation should immediately lead to shut-down to preclude catastrophic failure. Prolonged operation with these conditions would lead to significant wear of the seal faces, though wear is not considered in the seal model used herein.

Severe contact between the seal faces has long been suggested as a primary mechanism for seal failure; still, evidence for attributing seal failure to adverse contact conditions has previously been intuitive or experimental in nature. For the first time, Fig. 8 displays analytic evidence for failure-inducing contact in a flat-faced FMS seal, using waveforms of the minimum film thickness, frequency spectra, and axial asperity contact force between the faces. In this case, severe contact results from an instability caused by a lack of coning across the sealing dam, and is exacerbated by the large contact area between the seal faces. This flat-face condition is reasonable, considering that face coning is often generated via thermal deformation, which in turn is induced by viscous heat generation [12]. The thermal deformation time constant has been previously shown [12] to be several orders of magnitude higher than the period of seal rotation during lift-off or shut-down. Thus, FMS seals often operate for many revolutions prior to the appearance of significant face coning.

The minimum film thickness of the flat-faced during unstable operation is shown in Fig. 8a, where contact results primarily when the minimum film thickness is reduced below  $4\sigma$ . Once the instability has generated a sufficiently large dynamic response, the FMS seal transitions into a violent impact-rebound cycle, where the minimum film thickness becomes temporarily much larger than the desired set-point clearance  $C_0$ . Failure can then be attributed to several outcomes: excessive leakage or seal damage via severe contact forces (as shown in Fig. 8c). The aperiodic behavior of the seal motion at the onset of failure is evident in the frequency spectra, Fig. 8b.

Interestingly, no significant contact indicators were present in the seal's motion prior to failure ( $\tau < 850$ ). These results should serve as an additional motivator for always including coning in a mechanical face seal, as the taper caused by coning limits the contact pressure to a very localized area of the seal faces (and thus, the contact forces are small even if the localized contact pressures are large).

#### 4 Conclusions

Mechanical face seals are incredibly complex mechanisms where a proper design requires knowledge of lubrication, seal dynamics, and thermal effects, among others. This complexity in design, along with uncertainties in operation, manufacturing, and installation, results in a machine component which has previously been described as the most unpredictable machine element. Experimental, industrial, and intuitive experience led previous researchers and practitioners to venture undesirable seal face contact as a possible route to failure. For the first time, this work investigates analytically the problem of seal face contact as a condition present during steady-state operation. In some cases, particularly for large seal face coning and small misalignments, the FMS seal face response with contact qualitatively resembles that encountered during non-contacting operation; in these cases, reliably detecting the onset of contact may be difficult, and as a consequence prolonged operation may result in damage to the inner radius surface of the seal ring. In other cases involving coned-face FMS seals, the contact was observed to generate a significant nonlinear aperiodic response, the hallmark signatures of which could be used to quickly diagnose contact to the seal faces. In the most extreme case, a flat-faced seal was observed to quickly suddenly and catastrophically evolve into a response where extreme deflections and contact forces would assuredly result in expedient seal failure. In such a case, failure occurred so quickly that no current condition monitoring could permit the machine to be shut down prior to failure; thus, to avoid this scenario the designer should include some initial coning apart from that generated via thermal deformation.

Still, much work remains towards understanding dynamic contact between the faces of a hydrodynamic mechanical face seal. First, this work did not account for shaft speed or pressure differential transients which are encountered during system start-up and shut-down. Understanding seal behavior during these regimes is critical towards better designs avoiding

contact and better diagnostics to quickly detect contact when it does occur. In a similar manner, other researchers have shown that thermal deformations during these transients is an integral component of seal operation; the present study should be expanded to include heat generation due to viscous and friction effects, and then provide a method for using those effects to determine the transient coning of the seal.

### Nomenclature

$d$  Surface separation distance.  
 $h(r, \theta, t)$  Sealing dam film thickness.  
 $m$  Flexibly-mounted stator mass.  
 $n$  Rotor shaft speed.  
 $r$  Radial location coordinate.  
 $r_b$  Seal ring balance radius.  
 $r_i$  Inner seal ring radius.  
 $r_o$  Outer seal ring radius.  
 $u_z$  Seal ring axial deflection.  
 $z$  Asperity height.  
 $C_0$  Set-point centerline clearance.  
 $D_s$  Angular damping coefficient.  
 $D_{sz}$  Axial damping coefficient.  
 $E$  Composite elastic modulus.  
 $F_{cls}$  Closing force.  
 $F_{spr}$  Radial spring force.  
 $H$  Material hardness.  
 $I_t$  Flexibly-mounted stator mass moment of inertia.  
 $K_s$  Angular stiffness coefficient.  
 $K_{sz}$  Axial stiffness coefficient.  
 $N$  Areal density of asperities.  
 $P_i$  Inner fluid pressure.  
 $P_o$  Outer fluid pressure.  
 $R$  Surface height standard deviation.  
 $R_r$  Rotor radius.  
 $S_y$  Yield strength.  
 $\beta$  Flexibly-mounted stator seal coning angle.  
 $\xi\eta\zeta$  Inertial reference frame.  
 $\gamma_\xi$  Angular tilt about  $\xi$ .  
 $\gamma_\eta$  Angular tilt about  $\eta$ .  
 $\gamma_r$  Rotor tilt run-out.  
 $\gamma_s$  Magnitude of flexibly-mounted stator tilt.  
 $\gamma_{si}$  Static stator misalignment tilt.  
 $\mu$  Fluid viscosity.  
 $\nu$  Poisson ratio.  
 $\psi$  Plasticity index.  
 $\psi_s$  Stator precession.  
 $\psi_r$  Rotor precession.  
 $\sigma$  Surface height standard deviation.  
 $\sigma_s$  Asperity height standard deviation.  
 $\theta$  Circumferential position.  
 $\omega$  Asperity interference.  
 $\omega_c$  Critical interference.

### References

- [1] Etsion, I., 1982. "A Review of Mechanical Face Seal Dynamics". *The Shock and Vibration Digest*, **14**, pp. 9 – 14.
- [2] Green, I., and Bair, S., 1991. "Dynamic Response to Axial Oscillation and Rotating Seat Runout in Contacting Mechanical Face Seals". *Tribology Transactions*, **34**, pp. 169 – 176.
- [3] Lebeck, A. O., 1991. *Principles and Design of Mechanical Face Seals*. Wiley Interscience.
- [4] Burton, R. A., 1980. "Thermal Deformation in Frictionally Heated Contact". *Wear*, **59**, pp. 1 – 20.

- [5] Kennedy, F. E., and Hussaini, S. Z., 1987. "Thermo-Mechanical Analysis of Dry Sliding Systems". *Computers and Structures*, **26**, pp. 345 – 355.
- [6] Roberts, W. H., 1981. "Tribology in nuclear power generation". *Tribology International*, **14**(1), pp. 17 – 28.
- [7] Steinetz, B. M., Hendricks, R. C., and Munson, J., 1998. Advanced seal technology role in meeting next generation turbine engine goals. Tech. rep., National Aeronautics and Space Administration, Lewis Research Center.
- [8] Etsion, I., 1980. "Squeeze Effects in Radial Face Seals". *Journal of Lubrication Technology*, **102**, pp. 145 – 151.
- [9] Etsion, I., 1980. "The Accuracy of the Narrow Seal Approximation in Analyzing Radial Face Seals". *ASLE Transactions*, **22**, pp. 208 – 216.
- [10] Green, I., and Etsion, I., 1986. "A Kinematic Model for Mechanical Seals with Antirotation Locks or Positive Drive Devices". *Journal of Tribology*, **108**, pp. 42 – 45.
- [11] Ruan, B., Salant, R. F., and Green, I., 1997. "A Mixed Lubrication Model of Liquid/Gas Mechanical Face Seals". *Tribology Transactions*, **40**, pp. 647 – 657.
- [12] Green, I., 2002. "A Transient Dynamic Analysis of Mechanical Seals Including Asperity Contact and Face Deformation". *Tribology Transactions*, **45**(3), pp. 284 – 293.
- [13] Jang, J. Y., and Khonsari, M. M., 2000. "Thermoelastic Instability with Consideration of Surface Roughness and Hydrodynamic Lubrication". *Journal of Tribology*, **122**, pp. 725 – 732.
- [14] Etsion, I., and Harp, G., 2002. "A Laser Surface Textured Hydrostatic Mechanical Seal". *Tribology Transactions*, **45**(3), pp. 430 – 434.
- [15] Etsion, I., and Constantinescu, I., 1984. "Experimental Observation of the Dynamic Behavior of Noncontacting Coned-Face Mechanical Seals". *ASLE Transactions*, **27**(3), pp. 263 – 270.
- [16] Lee, A. S., and Green, I., 1994. "Higher Harmonic Oscillations in a Non-contacting FMR Mechanical Face Seal Test Rig". *Journal of Vibration and Acoustics*, **116**, pp. 161 – 167.
- [17] Harp, S. R., and Salant, R. F., 1998. "Analysis of Mechanical Seal Behavior During Transient Operation". *Journal of Tribology*, **120**, pp. 191 – 197.
- [18] Zou, M., Dayan, J., and Green, I., 2000. "Dynamic Simulation and Monitoring of a Non-Contacting Flexibly Mounted Rotor Mechanical Face Seal". *Proceedings of the Institution of Mechanical Engineers, Part C: Journal of Mechanical Engineering Science*, **214**(9), pp. 1195 – 1206.
- [19] Anderson, W., Jarzynski, J., and Salant, R. F., 2000. "Condition Monitoring of Mechanical Seals: Detection of Film Collapse Using Reflected Ultrasonic Waves". *Proceedings of the Institution of Mechanical Engineers, Part C: Journal of Mechanical Engineering Science*, **214**(9), pp. 1187 – 1194.
- [20] Reddyhoff, T., Dwyer-Joyce, R. S., and Harper, P., 2008. "A New Approach for the Measurement of Film Thickness in Liquid Face Seals". *Tribology Transactions*, **51**, pp. 140 – 149.
- [21] Jiao, J., Liu, W., Zhang, J., Zhang, Q., He, C., and Wu, B., 2013. "Time-frequency Analysis for Ultrasonic Measurement of Liquid-Layer Thickness". *Mechanical Systems and Signal Processing*, **35**, pp. 69 – 83.
- [22] Huang, W., Lin, Y., Liu, Y., Liu, X., Gao, Z., and Wang, Y., 2013. "Face Rub-Impact Monitoring of a Dry Gas Seal Using Acoustic Emission". *Tribology Letters*, **52**, pp. 253 – 259.
- [23] Zhang, Z., and Li, X., 2014. "Acoustic Emission Monitoring for Film Thickness of Mechanical Seals Based on Feature Dimension Reduction and Cascaded Decision". In Sixth International Conference on Measuring Technology and Mechatronics Automation.
- [24] Heshun, W., Zepei, H., and Chening, Z., 2009. "Fuzzy Recognition on the Working State of Noncontacting Mechanical Seals". In 2009 ISECS International Colloquium on Computing, Communication, Control, and Management.
- [25] Zou, M., and Green, I., 1999. "Clearance Control of a Mechanical Face Seal". *Tribology Transactions*, **42**(3), pp. 535 – 540.
- [26] Dayan, J., Zou, M., and Green, I., 1999. "Contact Elimination in Mechanical Face Seals Using Active Control". In Proceedings of the 7th IEEE Mediterranean Conference on Control and Automation.
- [27] Yelma, S. S., Miller, B. A., and Landers, R. G., 2006. "Clearance Regulation of Mechanical Gas Face Seals: Part II - Analysis and Control". *Tribology Transactions*, **49**, pp. 373 – 386.
- [28] Zhang, H., Landers, R. G., and Miller, B. A., 2010. "Adaptive Control of Mechanical Gas Face Seals with Rotor Runout and Static Stator Misalignment". *Journal of Dynamic Systems, Measurement, and Control*, **132**, pp. 041009.1 – 10.
- [29] Chang, W. R., Etsion, I., and Bogy, D. B., 1987. "An Elastic-Plastic Model for the Contact of Rough Surfaces". *Journal of Tribology*, **109**, pp. 257 – 263.
- [30] Minet, C., Brunetiere, N., and Tournerie, B., 2011. "A Deterministic Mixed Lubrication Model for Mechanical Seals". *Journal of Tribology*, **133**, pp. 042203.1–11.
- [31] Green, I., and Etsion, I., 1986. "Nonlinear Dynamic Analysis of Noncontacting Coned-Face Mechanical Seals". *ASLE Transactions*, **29**(3), pp. 383 – 393.
- [32] Green, I., 1989. "Gyroscopic and Support Effects on the Steady-State Response of a Noncontacting Flexibly-Mounted Rotor Mechanical Face Seal". *Journal of Tribology*, **111**, pp. 200 – 208.
- [33] Green, I., 1990. "Gyroscopic and Damping Effects on the Stability of a Noncontacting Flexibly-Mounted Rotor Me-

- chanical Face Seal”. In *Dynamics of Rotating Machinery*, pp. 153 – 157.
- [34] Green, I., and Etsion, I., 1986. “Pressure and Squeeze Effects on the Dynamic Characteristics of Elastomer O-Rings Under Small Reciprocating Motion”. *Journal of Tribology*, **108**, pp. 439 – 444.
- [35] Green, I., 2008. “On the Kinematic and Kinetics of Mechanical Seals, Rotors, and Wobbling Body”. *Mechanism and Machine Theory*, **43**, pp. 909–917.
- [36] Varney, P., and Green, I., 2014. “Nonlinear Phenomena, Bifurcations, and Routes to Chaos in an Asymmetrically Supported Rotor-Stator Contact System”. *Journal of Sound and Vibration*, **336**, pp. 207 – 226.
- [37] Sharoni, A., and Etsion, I., 1980. “Performance of End-Face Seals with Diametral Tilt and Coning - Hydrodynamic Effects”. *ASLE Transactions*, **24**(1), pp. 61 – 70.
- [38] Green, I., 1987. “The Rotor Dynamic Coefficients of Coned-Face Mechanical Seals with Inward or Outward Flow”. *Journal of Tribology*, **109**, pp. 129 – 135.
- [39] Payvar, P., and Salant, R. F., 1992. “A Computational Method for Cavitation in a Wavy Mechanical Seal”. *Journal of Tribology*, **114**, pp. 199 – 204.
- [40] Bair, S., Green, I., and Bhushan, B., 1991. “Measurement of Asperity Temperature of a Read/Write Head Slider Bearing in Hard Magnetic Recording Disks”. *Journal of Tribology*, **113**, pp. 547 – 554.
- [41] Patir, N., and Cheng, H. S., 1978. “An average flow model for determining effects of three-dimensional roughness on partial hydrodynamic lubrication”. *Journal of Tribology*, **100**, pp. 12 – 17.
- [42] Greenwood, J. A., and Williamson, J. B. P., 1966. “Contact of Nominally Flat Surfaces”. *Proceedings of the Royal Society of London A*, **295**, pp. 300 – 319.
- [43] Varney, P., and Green, I., 2015. “Rough Surface Contact of Curved Conformal Surfaces: An Application to Rotor-Stator Rub”. *Journal of Tribology*, (*accepted for publication*).
- [44] Jackson, R. L., and Green, I., 2006. “A statistical model of elasto-plastic asperity contact between rough surfaces”. *Tribology International*, **39**, pp. 906 – 914.
- [45] Jackson, R. L., and Green, I., 2005. “A Finite Element Study of Elasto-Plastic Hemispherical Contact”. *Journal of Tribology*, **127**, pp. 343 – 354.
- [46] Green, I., 2005. “Poisson Ratio Effects and Critical Values in Spherical and Cylindrical Hertzian Contact”. *International Journal of Applied Mechanics and Engineering*, **10**(3), pp. 451 – 462.
- [47] Etsion, I., 1982. “Dynamic Analysis of Noncontacting Face Seals”. *Journal of Tribology*, **104**(4), pp. 460 – 468.
- [48] Zou, M., Dayan, J., and Green, I., 2000. “Feasibility of Contact Elimination of a Mechanical Face Seal Through Clearance Adjustment”. *Journal of Engineering for Gas Turbines and Power*, **122**, pp. 478 – 484.

## Appendix A

The surface roughness parameters used herein are provided in Table 1, while the seal parameters are given in Table 2. The angular stiffness and damping coefficients are found according to Green and Etsion [10]. The balance radius  $r_b$  is obtained by balancing the opening and closing forces on the seal given a set-point desired clearance  $C_o$ . Lastly, the surface yield strength is found using a specified plasticity index, according to the procedure established by Jackson and Green [45].

List of Figures

1	Schematic of a flexibly-mounted stator mechanical face seal. . . . .	12
2	Reference frames used to model the flexibly-mounted stator mechanical face seal. . . . .	13
3	Contact between two rough surfaces is reduced to that of contact between a rigid flat and a composite rough surface. . . . .	14
4	Validation versus the results provided by Green and Etsion [10]. . . . .	15
5	Comparison of coned-face FMS minimum film thickness with and without contact (Parameter Set 1: $\gamma_r = 2$ mrad, $\gamma_{si} = 5$ mrad, $n = 1000$ rad/s). The 'no-contact' case considers a surface height standard deviation $\sigma = 1(10)^{-7}m$ , which does not generate contact with these operating conditions. . . . .	16
6	Example contact pressure and fluid pressure profiles for parameters provided in Appendix A ( $n = 1000$ rad/s)	17
7	FMS response to heavy contact (Parameter Set 2: $\gamma_r = 1$ mrad, $\gamma_{si} = 5$ mrad, $n = 2000$ rad/s) . . . . .	18
8	Severe contact condition in a flat-faced seal. Parameters used are found in Set 1 except for the coning, which is set as $\beta = 0$ ( $\gamma_r = 2$ mrad, $\gamma_{si} = 5$ mrad, $n = 1000$ rad/s). . . . .	19

Accepted Manuscript Not Copyedited

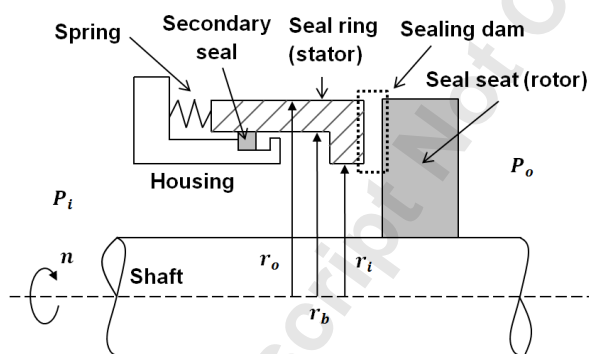


Fig. 1: Schematic of a flexibly-mounted stator mechanical face seal.

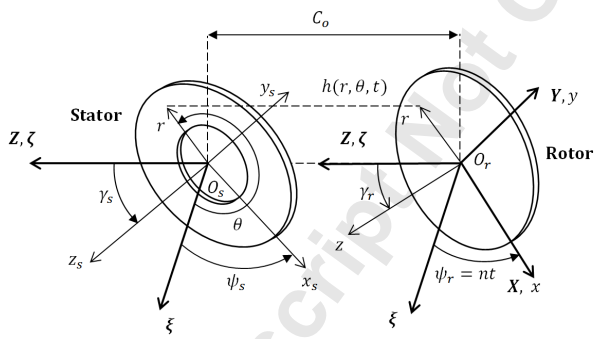


Fig. 2: Reference frames used to model the flexibly-mounted stator mechanical face seal.

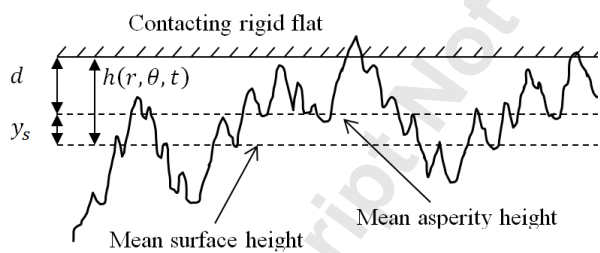


Fig. 3: Contact between two rough surfaces is reduced to that of contact between a rigid flat and a composite rough surface.

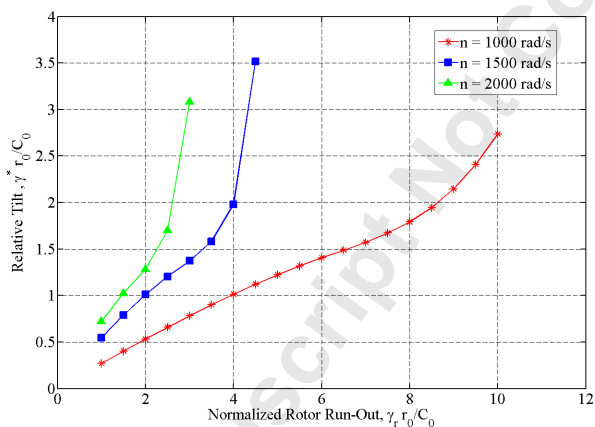
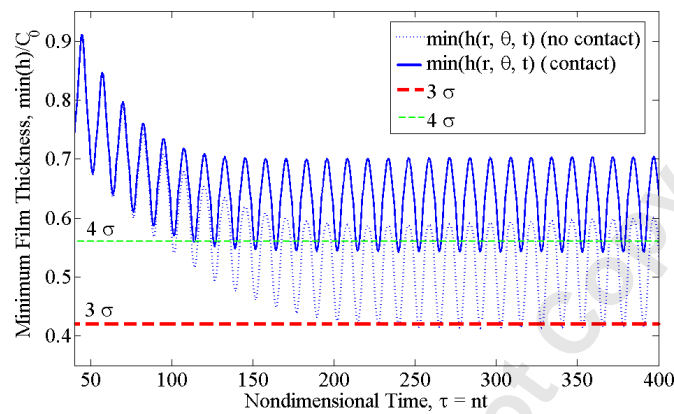
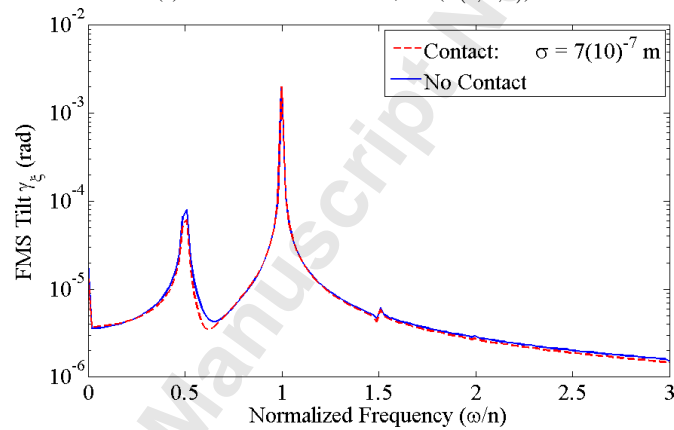


Fig. 4: Validation versus the results provided by Green and Etsion [10].

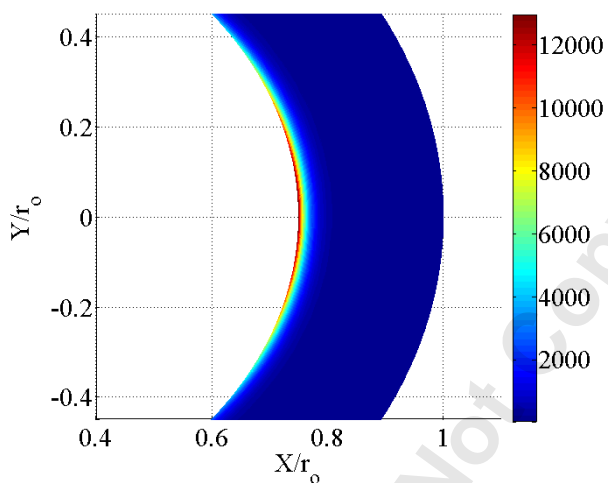


(a) Minimum film thickness,  $\min(h(r, \theta, t))$

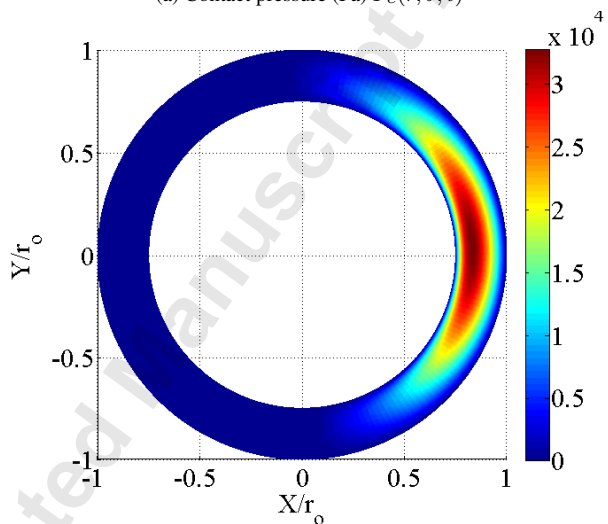


(b) Frequency content of steady-state FMS tilt  $\gamma_\xi$  (similar frequency content is seen in  $\gamma_\eta$ )

Fig. 5: Comparison of coned-face FMS minimum film thickness with and without contact (Parameter Set 1:  $\gamma_r = 2$  mrad,  $\gamma_{si} = 5$  mrad,  $n = 1000$  rad/s). The 'no-contact' case considers a surface height standard deviation  $\sigma = 1(10)^{-7}m$ , which does not generate contact with these operating conditions.

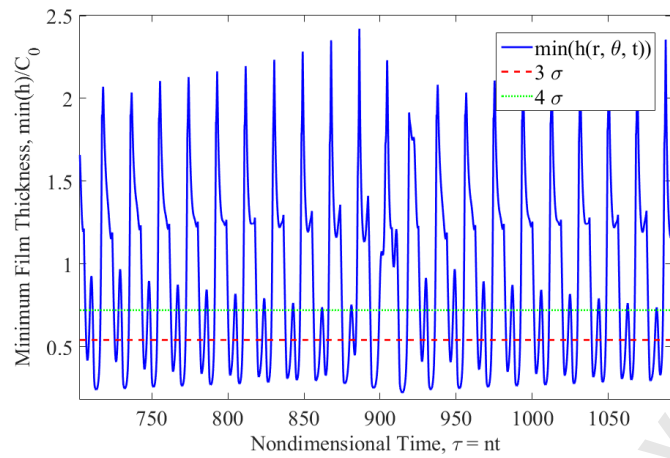


(a) Contact pressure (Pa)  $P_c(r, \theta, t)$

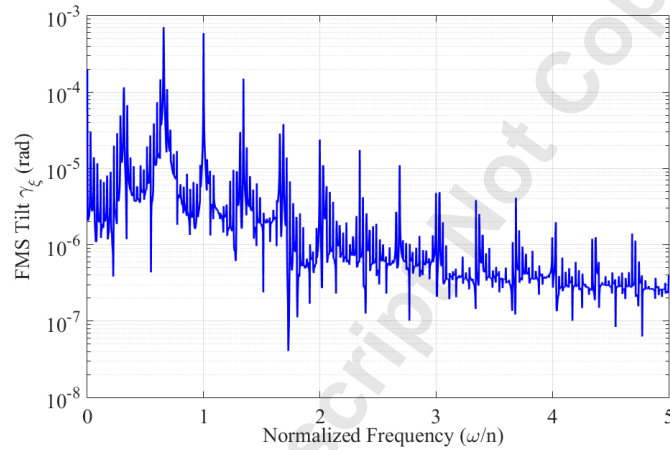


(b) Fluid film pressure (MPa),  $P_f(r, \theta, t)$

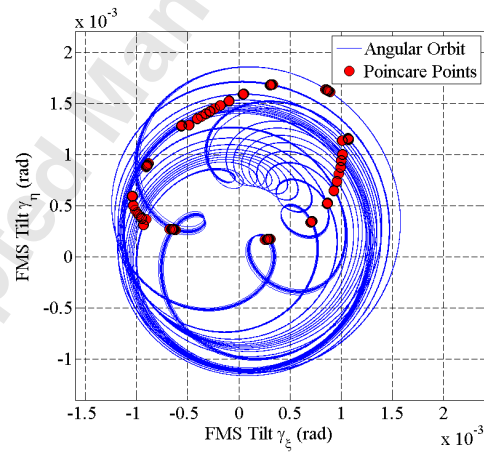
Fig. 6: Example contact pressure and fluid pressure profiles for parameters provided in Appendix A ( $n = 1000$  rad/s)



(a) Minimum film thickness,  $\min(h(r, \theta, t))$

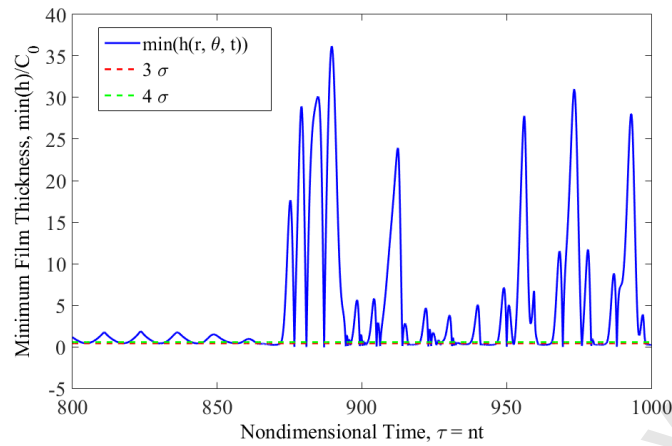


(b) Frequency content of steady-state FMS tilt  $\gamma_\epsilon$  (similar frequency content is seen in  $\gamma_\eta$ )

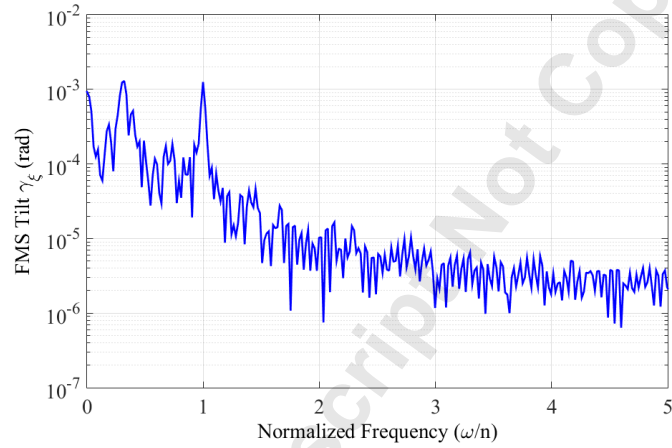


(c) Angular orbit and Poincaré section

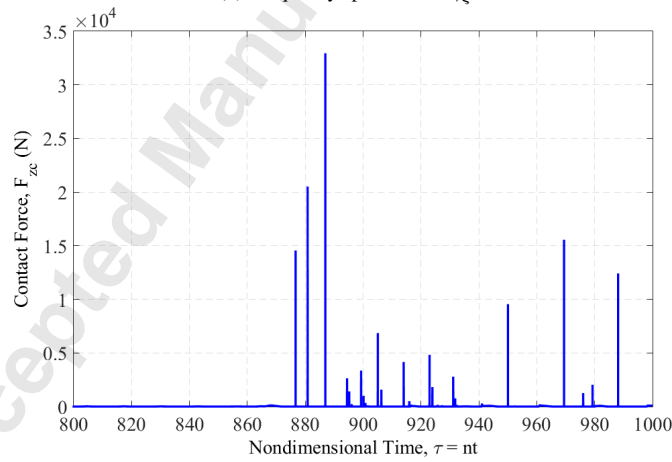
Fig. 7: FMS response to heavy contact (Parameter Set 2:  $\gamma_r = 1$  mrad,  $\gamma_{si} = 5$  mrad,  $n = 2000$  rad/s)



(a) Minimum film thickness  $h(r, \theta, t)/C_0$



(b) Frequency spectrum of  $\gamma_\xi$



(c) Axial contact force,  $F_{zc}$

Fig. 8: Severe contact condition in a flat-faced seal. Parameters used are found in Set 1 except for the coning, which is set as  $\beta = 0$  ( $\gamma_r = 2$  mrad,  $\gamma_{si} = 5$  mrad,  $n = 1000$  rad/s).

**List of Tables**

1	Surface parameters . . . . .	21
2	Seal parameters . . . . .	22

Accepted Manuscript Not Copyedited

Parameter	Set 1	Set 2
Plasticity index, $\psi_p$	5	5
Equivalent Modulus, $E$ (Pa)	$24(10)^9$	$24(10)^9$
Surface Stand. Dev., $\sigma$ (m)	$7(10)^{-7}$	$9(10)^{-7}$
Asperity Density, $\eta$ (asp./m <sup>2</sup> )	$4.2(10)^{11}$	$4.2(10)^{11}$
Asperity Radius, $R$ (m)	$1.7(10)^{-6}$	$1.7(10)^{-6}$

Table 1: Surface parameters

Parameter	Set 1	Set 2
Mass, $m$ (kg)	1.5	1.5
Axial Stiffness, $K_{sz}$ (N/m)	$1(10)^5$	$5(10)^5$
Axial Damping, $D_{sz}$ (N • s/m)	300	300
Radius of Gyration, $r_g$ (m)	0.04	0.04
Inner Radius, $r_i$ (m)	0.03	0.03
Outer Radius, $r_o$ (m)	0.04	0.04
Spring Force, $F_{spr}$ (N)	20	20
Inner Pressure, $P_i$ (kPa)	100	100
Outer Pressure, $P_o$ (kPa)	500	400
Coning, $\beta$ (mrad)	0.1	0.8
Clearance, $C_0$ ( $\mu m$ )	5	5
Viscosity, $\mu$ (mPa • s)	0.5	0.8

Table 2: Seal parameters